Journal of
Water, Sanitation & Hygiene for Development

IWA PUBLISHING

 Journal of Water, Sanitation and Hygiene for Development Vol 14 No 7, 552 doi: 10.2166/washdev.2024.025

Research Paper

Exploring the *Dipteryx alata* fruit endocarp as a novel source for the synthesis of silver nanoparticles: antibacterial and photocatalytic insights for water purification

Eduardo Beraldo de Morais[a,b,*], Marielle Xavier Nascimento[b], Leonardo Gomes de Vasconcelos[b,c], Rossean Golin[a], Paulo Renato Matos Lopes[d], Jéssica Aparecida Ribeiro Ambrosio[e] and Andreza Ribeiro Simioni[e]

[a] Postgraduate Program in Water Resources, Department of Sanitary and Environmental Engineering, Federal University of Mato Grosso, Cuiabá, MT, Brazil
[b] Federal University of Mato Grosso, Cuiabá, MT, Brazil
[c] Department of Chemistry, Federal University of Mato Grosso, Cuiabá, MT, Brazil
[d] Department of Plant Production, College of Agricultural and Technological Sciences, São Paulo State University, Dracena, SP, Brazil
[e] Research and Development Institute, Vale do Paraíba University, São José dos Campos, SP, Brazil
*Corresponding author. E-mail: eduardo.morais@ufmt.br

ABSTRACT

A simple, rapid, and non-toxic method was developed to synthesize silver nanoparticles (AgNPs) using an aqueous extract from the endocarp of Dipteryx alata fruit (DAE), a tree species native to the Brazilian Cerrado. The synthesis involved mixing DAE with a solution of $AgNO_3$ (2 mM) at room temperature. AgNPs synthesis was confirmed through detection of the surface plasmon resonance band at 421 nm. Characterization revealed spherical AgNPs with an average diameter of 137.5 $\pm$ 59.3 nm. FTIR analysis confirmed phytochemical involvement in AgNPs reduction and capping, while XRD analysis indicated their crystalline nature with a face-centered cubic structure. AgNPs exhibited antibacterial activity against *Escherichia coli* and *Enterococcus faecalis*, with zones of inhibition ranging from 10–4 mm for E. coli and 9–13 mm for *E. faecalis*, indicating sensitivity to AgNPs. Photocatalytic activity against rhodamine B (RhB) resulted in 99.3% removal in 180 min, with a degradation rate constant of 0.034 L mg^{-1} min^{-1} based on pseudo second-order kinetics. Phytotoxicity studies confirmed the non-toxic nature of degraded RhB products on *Cucumis sativus*. These findings highlight the potential of AgNPs from DAE extract in antibacterial and dye remediation applications.

Key words: green synthesis, photocatalytic degradation, phytotoxicity, textile dyes, water purification

HIGHLIGHTS

- Silver nanoparticles (AgNPs) were synthesized using *Dipteryx alata* fruit endocarp.
- Antibacterial properties of AgNPs were validated against *Escherichia coli* and *Enterococcus faecalis*.
- The photocatalytic activity of the AgNPs was confirmed by studying the degradation of rhodamine B.
- Phytotoxicity studies with *Cucumis sativus* confirmed the non-toxic nature of the degraded products of rhodamine B.
- The synthesized AgNP is promising for water treatment.

GRAPHICAL ABSTRACT

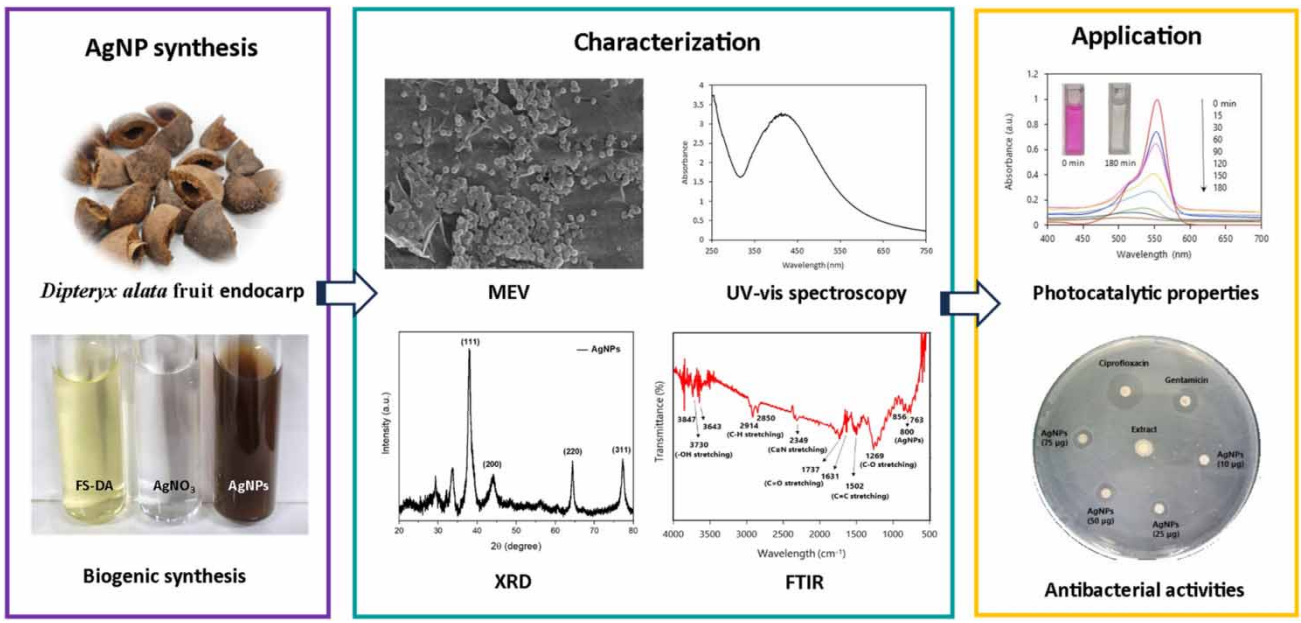

1. INTRODUCTION

Nanotechnology is a rapidly advancing field focused on manipulating and utilizing materials at the nanoscale. Within this domain, metallic nanoparticles (MNPs) have garnered significant attention due to their unique properties, such as a high surface area-to-volume ratio, enhanced reactivity, and distinct optical and magnetic characteristics (Manikandan *et al.* 2021; Azeez *et al.* 2023). These attributes make MNPs highly desirable for various applications across electronics, medicine, materials science, energy, and environmental remediation (Singh *et al.* 2019; Nguyen *et al.* 2020; Abbas & Amin 2022; Hossain *et al.* 2022).

Silver, gold, platinum, iron, and copper are among the commonly used metals for nanoparticle synthesis, owing to their inherent properties and chemical stability. Notably, silver nanoparticles (AgNPs) have been a focal point of extensive research in recent years. AgNPs exhibit distinct optical characteristics attributed to surface plasmon resonance, along with noteworthy antimicrobial, catalytic, and electronic properties, making them highly sought after in various fields (Rafique *et al.* 2017; Abdelghany *et al.* 2018). In the medical field, AgNPs find applications in drug delivery systems, wound healing, and antibacterial coatings (Mousavi *et al.* 2018; Tarannum *et al.* 2019; Huq *et al.* 2022). They also play a crucial role in biosensors designed to detect biological molecules and environmental pollutants (Alex *et al.* 2020). AgNPs exhibit promising potential in combating multidrug-resistant bacteria, showcasing their value in antimicrobial therapy (Lakkim *et al.* 2020). Additionally, AgNPs find applications in water purification, serving as catalysts and acting as adsorbents for both organic and inorganic compounds (Dixit *et al.* 2018; Singh *et al.* 2019; Rohaizad *et al.* 2020).

Traditionally, MNPs are synthesized using chemical and physical methods, such as the reduction of metallic salts, thermal decomposition, co-precipitation, radiation-assisted methods, and pyrolysis (Ishak *et al.* 2019). However, these methods have drawbacks, including high energy requirements and the use of hazardous chemicals that can be harmful to human health and the environment (Rolim *et al.* 2019; Hawar *et al.* 2022). In contrast, biogenic methods for synthesizing MNPs have gained popularity due to their simplicity, cost-effectiveness, and the absence of toxic compounds. Furthermore, these methods can be conducted safely at room temperature and pressure (Sasikala *et al.* 2015; Rafique *et al.* 2017).

Various biological systems have been utilized for MNP synthesis, including plants, bacteria, fungi, and algae (Ishak *et al.* 2019; Saeed *et al.* 2020; Dadayya *et al.* 2023; Kingslin *et al.* 2023). Plant extracts are widely used due to the presence of phytocompounds such as terpenoids, flavonoids, alkaloids, saponins, and tannins, which act as reducing and stabilizing agents (Ishak *et al.* 2019). Recent studies have successfully employed several plant species, including *Carica papaya* (Jain *et al.* 2020), *Ctenolepis garcinia* (Narayanan *et al.* 2021), *Alhagi graecorum* (Hawar *et al.* 2022), *Ligustrum vulgare* (Singh & Mijakovic

2022), *Citrus limon* (Khane *et al.* 2022), and *Allium cepa* (Baran *et al.* 2023), for the synthesis of AgNPs. However, the synthesis of AgNPs utilizing the *Dipteryx alata* fruit endocarp (DAE) extract has not been previously explored. *D. alata* is a tree species native to the Brazilian Cerrado, belonging to the Fabaceae family. Its nuts, known as baru, are rich in fibers, healthy fats, vitamins, minerals, and antioxidants and are consumed in Brazil as roasted nuts or as an ingredient in typical gastronomy (Viana *et al.* 2023). The DAE is a woody residue discarded during the agro-industrial processing of the nuts and presents itself as a new source of phytochemicals for reducing and capping nanoparticles.

Given the imperative for developing sustainable nanoparticle synthesis methods, this study explored the utilization of DAE extract for the first-time synthesis of AgNPs. The synthesized AgNPs were characterized using various techniques such as UV–Vis spectroscopy, Fourier-transform infrared spectroscopy (FTIR), scanning electron microscopy (SEM), dynamic light scattering (DLS), and X-ray diffraction (XRD). Furthermore, the antibacterial activities of AgNPs were evaluated against *Escherichia coli* and *Enterococcus faecalis*, while their photocatalytic properties were tested for the degradation of rhodamine B (RhB) in an aqueous solution.

2. MATERIALS AND METHODS

2.1. Materials and chemicals

The DAE (Figure 1(a)) was obtained as waste from agroindustry in Mato Grosso State, Brazil, that processes the baru nuts. Silver nitrate ($AgNO_3$), sodium hydroxide (NaOH), and RhB ($C_{28}H_{31}ClN_2O_3$) were purchased from Synth, Brazil, and all chemical reagents were of analytical grade. Nutrient broth and Mueller–Hinton agar were purchased from Himedia Laboratories Ltd, India.

2.2. Preparation of the aqueous extract of DAE

The DAE was thoroughly washed with distilled water to remove impurities and then oven-dried at 60 °C for 48 h. It was subsequently finely shredded into particles smaller than 500 μm using a high-power grinder. To prepare the extract, a mixture of DAE and distilled water in a ratio of 1:100 (m/v) was stirred at 80 °C for 60 min (Singh *et al.* 2019). The resulting extract was separated through filtration and stored at 4 °C until further use.

2.3. Synthesis of biogenic AgNPs

The procedure for synthesizing biogenic AgNPs was developed based on methods described in the literature (Aisida *et al.* 2019; Hossain *et al.* 2022; Baran *et al.* 2023). Initially, 20 mL of the DAE extract was added to 100 mL of a silver nitrate solution (2 mM), and the pH of the mixture was adjusted to 10.0 using a dropwise addition of a NaOH solution (0.1 M). The reaction mixture was stirred in the dark for 1 h at room temperature. The volume of 20 mL of the DAE extract used for AgNP synthesis was selected as optimal after testing various volumes of DAE (1, 10, 20, and 50 mL). The development of a reddish-brown color from a light yellow mixture indicated the formation of AgNPs. The synthesized AgNPs were

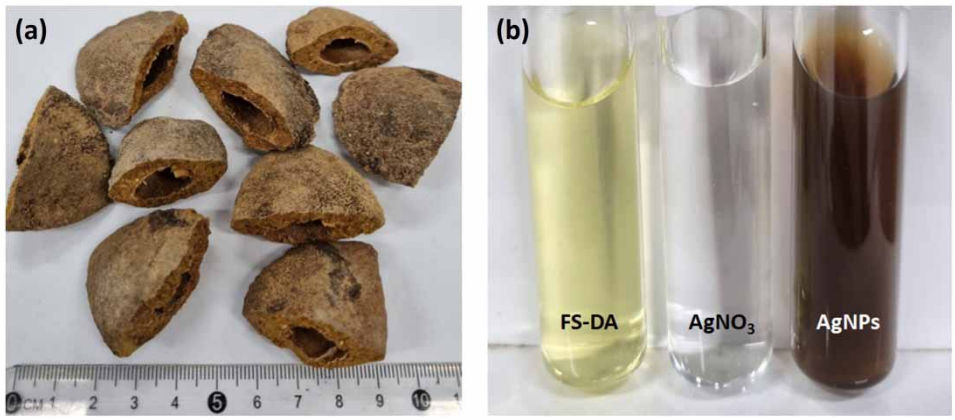

Figure 1 | DAE (a) and AgNP synthesis process: extract of *D. alata* (DAE extract), $AgNO_3$ solution, and AgNP colloidal solution (b).

collected by centrifugation (12,000 rpm, 15 min), washed twice with distilled water to remove ions and residues from the DAE extract, and dried in an oven at 105 °C for 2 h.

2.4. Characterization of AgNPs

The AgNPs were characterized using spectroscopic and imaging techniques. UV–Vis spectra were recorded from 250 to 750 nm with a resolution of 1.0 nm using a UV–Vis Hach DR 6000 spectrophotometer. FTIR analysis was conducted in the range of 500–4,000 cm^{-1} to identify the functional groups of phytochemicals responsible for stabilizing the nanoparticles. AgNP samples were prepared as KBr discs, and the spectra were acquired using a Shimadzu IRAffinity-1 spectrometer. The morphology of the AgNPs was investigated by SEM using a Zeiss EVO-MA10 instrument at an accelerating voltage of 20 kV, and the particle size and frequency distribution were confirmed by DLS (Malvern Zetasizer Nano ZS, Malvern, UK). The crystalline nature of the nanoparticles was determined by XRD analysis on a Bruker D8 Advance diffractometer. The analysis was performed with Cu Kα radiation, operating at a voltage of 40 kV and a current of 40 mA.

2.5. Assessment of antibacterial activity

The antibacterial activity of biogenic AgNPs was assessed against *E. coli* (ATCC 25922) and *E. faecalis* (ATCC 19433) using the disc diffusion method (Jain *et al.* 2020). Initially, bacterial strains were cultured in nutrient broth at 37 °C until reaching an optical density of 0.5 (at $\lambda = 600$ nm). Subsequently, bacterial suspensions were evenly spread on the surface of Mueller–Hinton agar plates using a sterile cotton swab. Five sterile discs were placed on each plate, and varying masses of AgNPs (10, 25, 50, and 75 μg) were applied to the discs. Discs containing ciprofloxacin (5 μg) and gentamicin (10 μg) served as positive controls. The plates were incubated at 37 °C, and after 24 h, the diameter of the inhibition zones was measured. The experiments were conducted in triplicate.

2.6. Photocatalytic activity

The photocatalytic activity of the AgNPs was assessed by studying the degradation of RhB under ultraviolet radiation. In the experiment, 20 mg of AgNPs was introduced into a 100 mL aqueous solution containing 25 mg L^{-1} of RhB. The dye solution was continuously agitated on a magnetic stirrer and exposed to UV light (15 W, 254 nm). The degradation of RhB was monitored at regular intervals using UV–Vis spectrophotometry.

2.7. Phytotoxicity of the degraded product of RhB

Cucumber seeds (*Cucumis sativus*, seed germination = 99%) were exposed to the degraded product of RhB to assess its toxicity, following the recommendation by the U.S. Environmental Protection Agency for toxicity testing and environmental assessment (U.S. EPA 1998). In Petri dishes (90 mm diameter), 10 seeds were positioned on filter paper moistened with 5 mL of the test solution. The plates were incubated at 22 °C for 120 h. Distilled water served as the negative control and all assays were performed in triplicate. Following the incubation period, the number of germinated seeds as well as the lengths of the radicle and hypocotyl were measured.

3. RESULTS AND DISCUSSION

3.1. Characterization of biogenic AgNPs

The change in the color of the $AgNO_3$ solution, transitioning from light yellow to reddish-brown upon mixing with the DAE extract, serves as the primary indicator of AgNP synthesis (Figure 1(b)). The UV–Vis spectrum of this mixture (Figure 2(a)) exhibits a distinct and strong absorption band at 421 nm, which is attributed to surface plasmon resonance, thereby confirming the formation of AgNPs (Narayanan *et al.* 2021). Similar AgNP bands within the 400–440 nm range were also observed in other studies that used leaf extracts of *Carissa carandas* L. (Singh *et al.* 2021), *Ocimum americanum* (Manikandan *et al.* 2021), and *Ctenolepis garcini* L. (Narayanan *et al.* 2021).

The FTIR analysis was conducted to evaluate the interaction between synthesized AgNPs and the phytochemicals in the extract. The absorption bands at 3,847, 3,730, and 3,643 cm^{-1} in the FTIR spectrum (Figure 2(b)) are likely attributed to the –OH stretching vibrations of phenols and alcohols (Singh *et al.* 2020). The bands at 2,914 and 2,850 cm^{-1} corresponded to C–H stretching vibrations and at 2,349 cm^{-1} to C ≡ N stretching vibrations (Singh *et al.* 2019). Bands at 1,737 and 1,631 cm^{-1} are associated with C = O stretching vibrations of aldehydes, ketones, and carboxylic acids (Sangaonkar & Pawar 2018). Furthermore, stretching vibrations of C = C and C–O at 1,502 and 1,269 cm^{-1}, respectively, were also observed (Ayinde *et al.* 2019). Particularly, the absorption bands at around 850–750 cm^{-1} indicated the bonding of AgNPs with oxygen

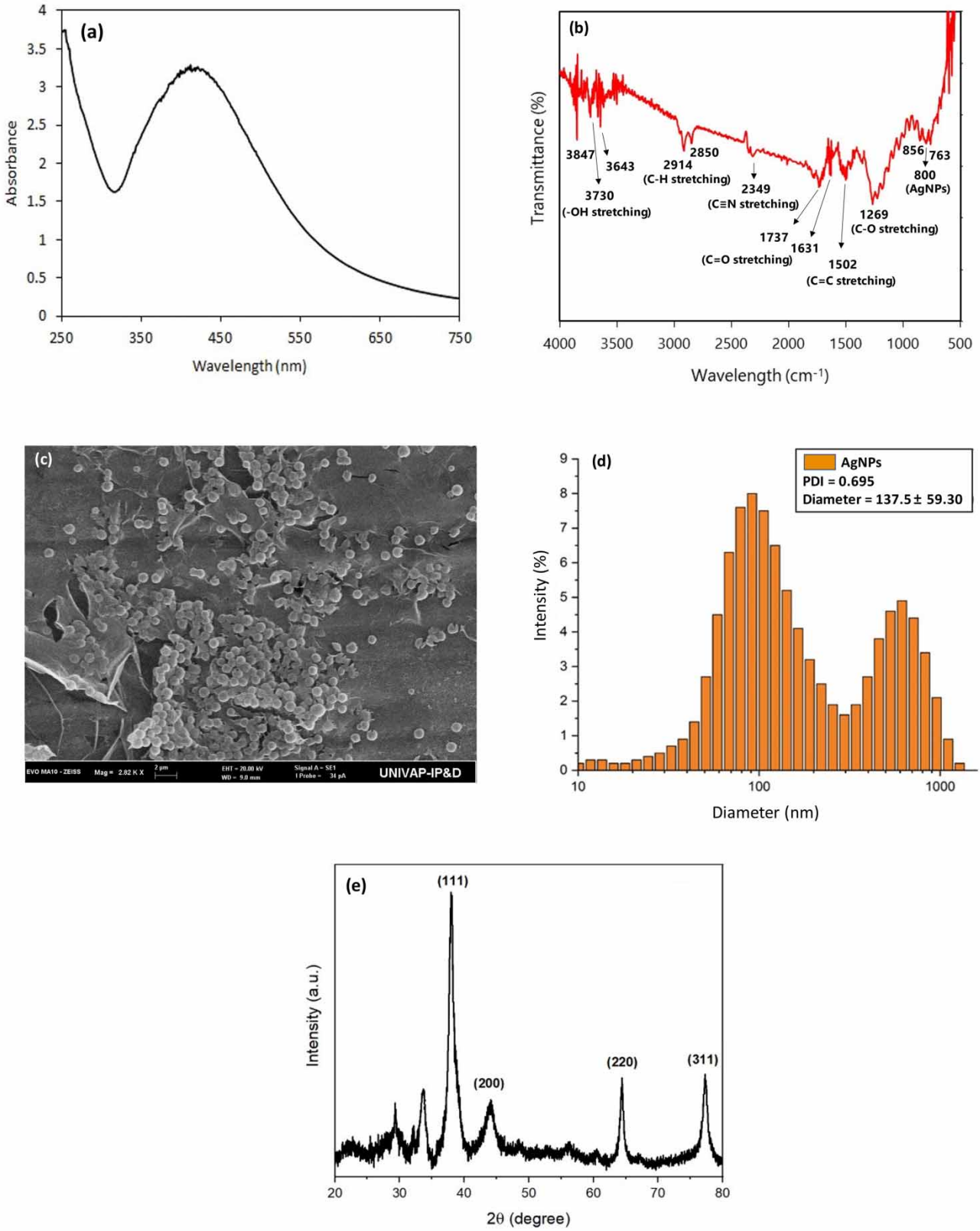

Figure 2 | UV–vis absorption spectrum (a), FTIR spectrum (b), SEM image (c), particle size distribution (d), and XRD analysis of AgNPs synthesized from the extract of DAE(e).

(Singh *et al.* 2019). Therefore, the FTIR analysis confirmed that the extract played a crucial role in reducing and capping AgNPs.

SEM was utilized to study the morphology of the AgNPs. As depicted in Figure 2(c), the nanoparticles exhibited a spherical shape with some degree of agglomeration, which was attributed to the interaction between biomolecules on the nanoparticle surface (Sasikala *et al.* 2015; Aisida *et al.* 2019).

The nanoparticle size distribution was determined from the DLS analysis (Figure 2(d)). The average particle size was 137.5 ± 59.3 nm with a polydispersity index (PDI) of 0.695. The PDI, ranging from 0 to 1, indicates the size uniformity of nanoparticles in a colloid suspension. PDI values ≤ 0.5 suggest that the samples are monodisperse, with nanoparticles having similar shapes and sizes (Majoumouo *et al.* 2019). Since the AgNPs had PDI values greater than 0.5, the nanoparticles can be classified as polydisperse.

XRD analysis confirmed the crystalline nature of AgNPs, with four main peaks observed in the XRD diffractogram (Figure 2(e)). These peaks at 2θ values of 37.96°, 44.10°, 64.38°, and 77.27° correspond to the (111), (200), (220), and (311) crystallographic planes, respectively, indicative of the face-centered cubic structure of AgNPs (Aisida *et al.* 2019). Two additional peaks were observed at 29.345° and 33.52°, potentially indicating the presence of organic compounds in the extract. Similar results were obtained in other studies (Aisida *et al.* 2019; Korkmaz *et al.* 2020; Nguyen *et al.* 2020).

3.2. Antibacterial activity of AgNPs

The antibacterial activity of AgNPs was tested against *E. coli* (Gram-negative) and *E. faecalis* (Gram-positive) bacteria. *E. coli* is a commensal bacterium that colonizes the intestines of warm-blooded animals and has been used as a fecal indicator in water and wastewater (Brum *et al.* 2016). Some strains can be pathogenic, causing urinary tract infections and intestinal diseases (Mare *et al.* 2021). *E. faecalis* is also a commensal bacterium in the gastrointestinal tracts of animals, including humans, and can cause a wide range of infections, including bloodstream infections, urinary tract infections, and endocarditis (Parthasarathy *et al.* 2021). As seen in Figure 3, zones of inhibition (ZOIs) were observed for the two bacterial strains, indicating the antibacterial activity of AgNPs. The DAE extract did not show any inhibitory effect. The diameters of the ZOI ranged from 10 to 14 mm for *E. coli* and 9 to 13 mm for *E. faecalis* (Table 1). The sensitivity to the antibacterial agent could be classified by the diameter of the ZOI as resistant (diameter < 8 mm), sensitive (diameter between 9 and 14 mm), very sensitive (diameter between 15 and 19 mm), and extremely sensitive (diameter > 20 mm) (Ponce *et al.* 2003). Thus, the bacterial strains evaluated are sensitive to AgNPs. The antibacterial properties of AgNPs synthesized in this investigation are in agreement with previous reports that used the aqueous *Citrus limon* extract (Khane *et al.* 2022) and aqueous *Ctenolepis garcinia* extract (Narayanan *et al.* 2021) to synthesize the AgNPs.

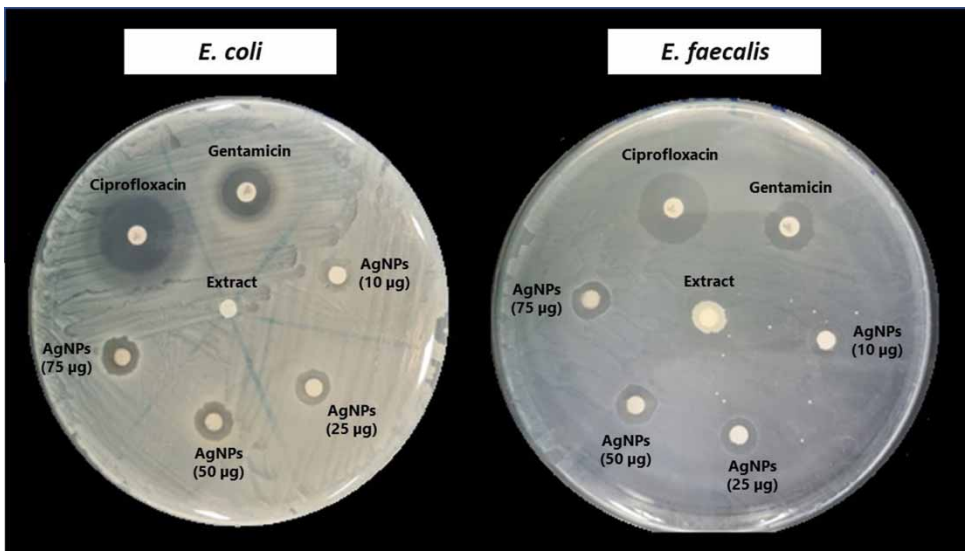

Figure 3 | Antibacterial activity of AgNPs against *E. coli* and *E. faecalis*.

Table 1 | Zone of inhibition (mm) of AgNPs against bacterial strains

Organisms	Ciprofloxacin	Gentamicin	Extract	AgNPs			
				10 μg	25 μg	50 μg	75 μg
E. coli	24 ± 0.6	15 ± 0.6	0	10 ± 1.2	11 ± 1.0	13 ± 1.5	14 ± 0.6
E. faecalis	22 ± 0.6	16 ± 1.2	0	9 ± 0.6	10 ± 2.1	13 ± 0	13 ± 1.5

The precise mechanisms underlying the antibacterial action of AgNPs are still under investigation. The main hypotheses suggest that AgNPs physically damage bacterial cell walls and membranes, leading to rupture, cellular content loss, and bacterial death (Tang & Zheng 2018). AgNPs may also penetrate bacteria and induce the formation of reactive oxygen species (ROS) that damage proteins, lipids, and nucleic acids (Aziz *et al.* 2015). These nanoparticles can also disrupt the electron transport chain, affecting energy production and reducing metabolic capacity (Singh *et al.* 2020).

3.3. Photocatalytic properties of AgNPs

The photocatalytic properties of AgNPs were investigated in terms of the degradation of RhB, a toxic dye widely used in the paper, textile, leather, and paint industries (Golin *et al.* 2022). The UV–Vis absorption spectrum for RhB degradation at different times is shown in Figure 4(a). An absorption band at 553 nm, which is related to the chromophore group of dyes belonging to the xanthene class, was observed (Wang *et al.* 2019). This band decreased over time and practically disappeared after 180 min, with RhB degradation reaching 99.3%. Experiments under UV irradiation without AgNPs and with AgNPs in dark conditions were also conducted (Figure 4(b)). Observations showed minimal degradation when the RhB solution was solely irradiated by UV (3.9%). When only the AgNPs were used in the dark, there was a removal rate of 22.7% of RhB, which can be attributed to adsorption by the nanoparticles.

The photocatalytic degradation data were evaluated using both first- and second-order kinetic models, as described by Equations (1) and (2) (Rohaizad *et al.* 2020):

$$\ln \frac{C_t}{C_0} = -k_1 t \tag{1}$$

$$\frac{1}{C_t} + \frac{1}{C_0} = k_2 t \tag{2}$$

where C_0 and C_t represent the concentrations of RhB (mg L^{-1}) at the beginning of the reaction and at time t (min), respectively. The parameter k_1 corresponds to the first-order rate constant, and k_2 is the second-order rate constant. The photocatalytic degradation data were best fitted by the second-order kinetic model ($R^2 = 0.980$, Figure 5(b)) compared to the first-order degradation kinetics ($R^2 = 0.915$, Figure 5(a)). The k_2 estimated by the second-order kinetic model was 0.037 L mg^{-1} min^{-1}.

The mechanism involved in the photocatalytic degradation of RhB by AgNPs is depicted in Figure 6. The degradation process occurs on the surface of AgNPs. When exposed to UV irradiation, electrons in the valence band (VB) become excited and transition to the conduction band (CB), generating electron (e^-_{CB})/hole (h^+_{VB}) pairs (Azeez *et al.* 2023). The e^-_{CB} electrons react with dissolved oxygen (O_2), leading to the formation of superoxide radical anions ($\cdot O_2^-$). Simultaneously, the h^+_{VB} holes interact with water molecules, producing hydroxyl radicals ($\cdot OH^-$). These highly reactive species are responsible for the degradation of RhB into smaller constituents, such as NH_4^+ , NO_3^- , CO_2, and H_2O (Shaikh *et al.* 2020).

The reusability of any photocatalyst is crucial for practical applications. After the optimal degradation of RhB, AgNPs were recovered using centrifugation, washed with distilled water, and utilized in multiple degradation reusability cycles (four cycles). In the first cycle, RhB degradation reached 99.5%, while 91.7% of RhB was degraded in the fourth cycle (Figure 7). Despite this reduction, the AgNPs maintained their high photocatalytic efficiency, highlighting their excellent photochemical stability.

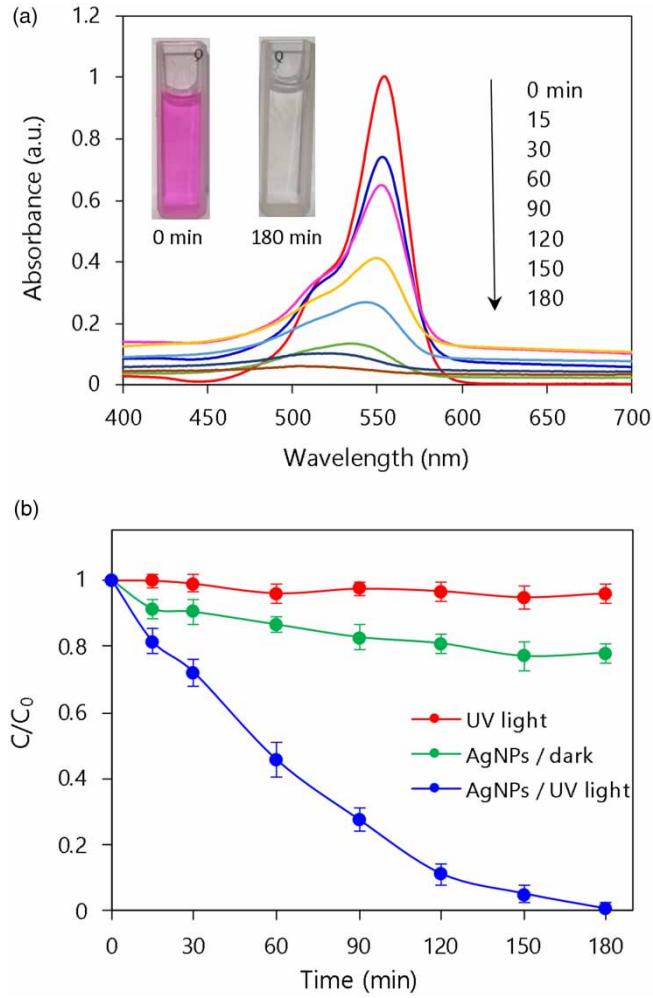

Figure 4 | UV–vis spectra of the photocatalytic degradation reaction of RhB dye using AgNPs as catalyst (a), and plot of C/C_0 against reaction time for the removal of RhB dye in the presence of AgNPs in the dark and under UV light (b).

3.3.1. Validation of RhB remediation

During the degradation of organic contaminants, it is expected that degraded products are non-toxic. Thus, toxicity tests were conducted with cucumber seeds (*C. sativus*) to assess the potential toxic effects of degraded RhB solution. Control (distilled water), RhB solution (25 mg L^{-1}), and degraded RhB solution allowed 100% germination (Table 2). However, the development of the seedlings was negatively affected by the undegraded RhB solution (Figure 8). The mean radicle length and hypocotyl lengths of *C. sativus* were 1.73 and 1.44 cm, respectively, in the RhB solution, while in distilled water, the radicle and hypocotyl lengths were 7.74 and 2.48 cm, respectively (Table 2). In the case of the degraded RhB solution, radicle and hypocotyl lengths of 7.54 and 2.13 cm were observed. Although the radicle and hypocotyl lengths of the degraded RhB solution were slightly lower compared to those in distilled water, statistical analysis (analysis of variance (ANOVA)) did not reveal any significant difference between them and the control. This suggests the absence of toxicity and validates the RhB remediation through the photocatalytic process using AgNPs. These results are consistent with the findings reported by Shaikh *et al.* (2020), who also observed that the products of the photocatalytic degradation of RhB by AgNPs showed no phytotoxicity to *Cicer arietinum*.

3.4. Application of AgNPs in water purification

Textile wastewater treatment presents significant environmental challenges due to the presence of various hazardous compounds, including dyes, heavy metals, and aromatic compounds. Annually, approximately 140,000 tons of dyes are

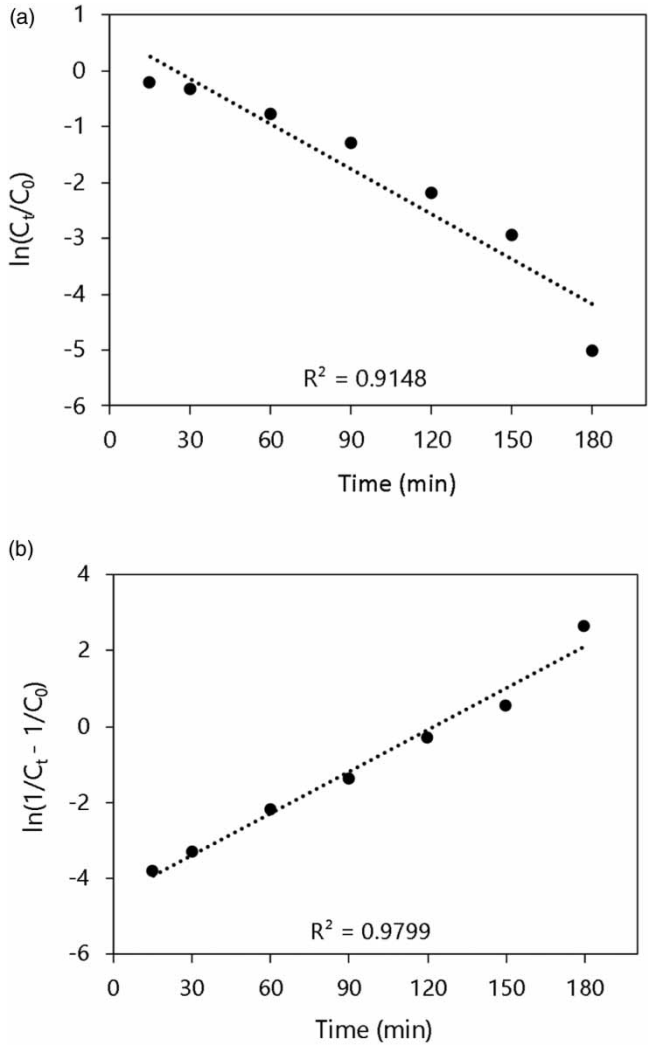

Figure 5 | Kinetic models for the photocatalytic degradation of RhB calculated using the first-order kinetic (a) and second-order kinetics models (b).

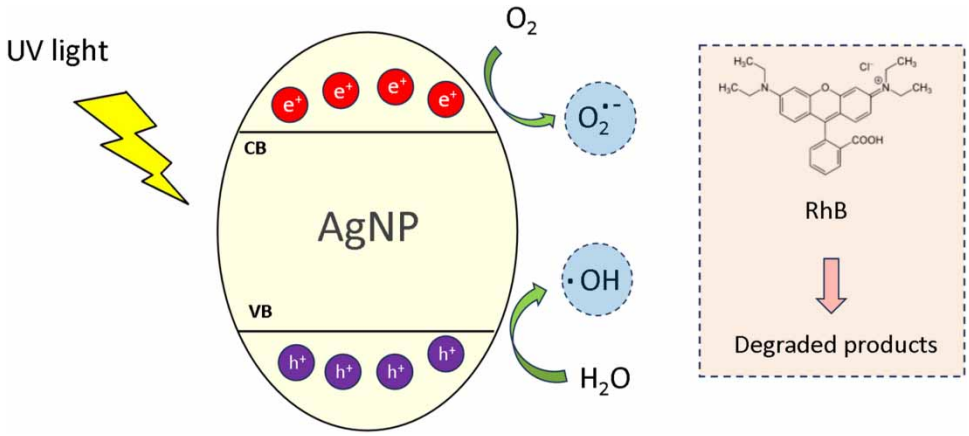

Figure 6 | Proposed mechanism for the photocatalytic degradation of RhB by AgNPs.

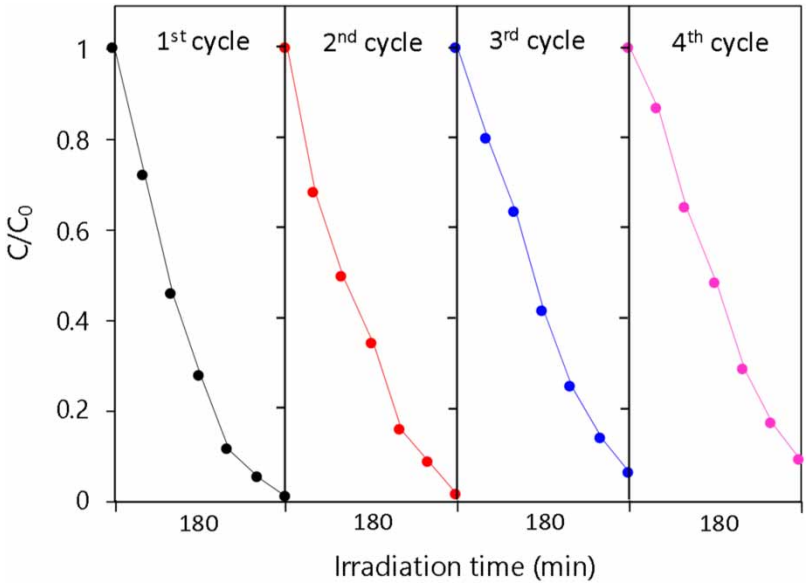

Figure 7 | Reusability of the AgNPs after four successive cycles of RhB degradation.

Table 2 | Phytotoxicity studies of RhB and its degraded products on *C. sativus* after photocatalytic degradation by AgNPs

Parameters studied	Control (distilled water)	RhB solution	Degraded RhB solution
Germination (%)	100	100	100
Radicle (cm)	7.74 ± 0.95	1.73 ± 0.50*	7.54 ± 0.85
Hypocotyl (cm)	2.48 ± 0.39	1.44 ± 0.37*	2.13 ± 0.25

Values are mean of three replicates (mean ± standard error).
*Significantly different from the control (seeds germinated in water) using ANOVA with the Tukey–Kramer multiple comparison test ($P < 0.05$).

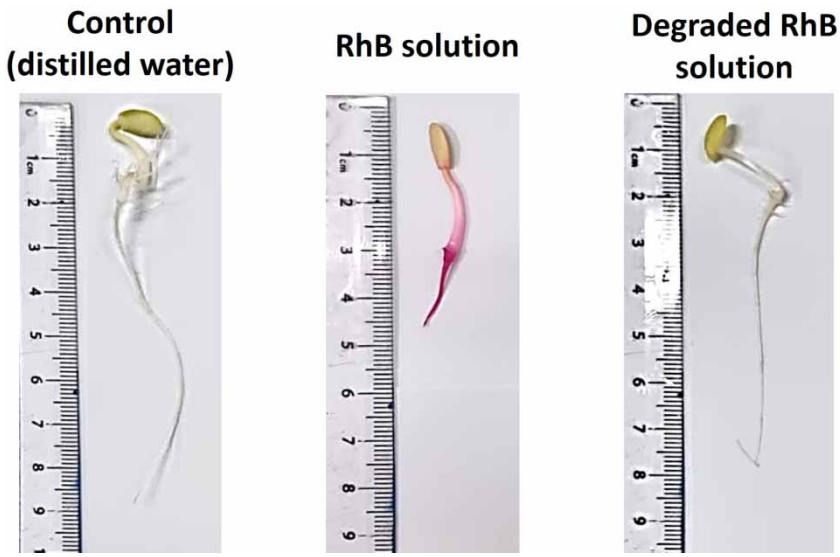

Figure 8 | Appearance of *Cucumis sativus* seedlings germinated in distilled water, RhB solution, and degraded RhB solution.

arbitrarily discharged into global water resources (Islam *et al.* 2023). These compounds can alter water color and transparency, reducing sunlight penetration and impeding photosynthesis, crucial for the growth of aquatic plants and algae (Golin *et al.* 2022). Additionally, many dyes contain toxic chemicals that can harm aquatic organisms, disrupting their physiological processes and leading to population declines (Castro *et al.* 2017). In our study, AgNPs synthesized from DAE effectively degraded RhB, offering a promising solution for removing dye pollutants from textile effluents. Given AgNPs' excellent photocatalytic activity against dyes, there is an opportunity to apply them for degrading other emerging contaminants such as pharmaceuticals, pesticides, and personal care products. This further expands their potential application in purifying industrial and urban wastewater. The ability of AgNPs to deactivate bacteria is another characteristic observed in this study that can be exploited for water disinfection. AgNPs have proven to be effective in eradicating over 700 microorganisms that are commonly encountered in sewage treatment plants (Epelle *et al.* 2022). Therefore, leveraging the potential of AgNPs in water purification emerges as a pivotal step toward tackling the urgent challenges of water contamination, providing a sustainable and efficient solution for ensuring water quality, safeguarding public health, and protecting the environment.

4. CONCLUSION

In this study, AgNPs were successfully synthesized using DAE, a residue from agroindustry. The characterization of these AgNPs involved various analytical techniques, including UV–Vis spectroscopy, FTIR, SEM, DLS, and XRD. The AgNPs exhibited a spherical shape with a diameter of 137.5 ± 59.3 nm and a PDI of 0.695, classifying them as polydisperse. FTIR analysis revealed that the phytochemicals present in the extract played a crucial role in reducing and capping the AgNPs. The crystalline nature of the AgNPs was confirmed through XRD analysis, showing characteristic peaks corresponding to the face-centered cubic structure of silver. Notably, these AgNPs demonstrated significant antibacterial activity against *E. coli* and *E. faecalis*. The photocatalytic properties of the AgNPs were evaluated by their ability to degrade RhB, achieving a 99.3% degradation of this dye. The kinetics of this photocatalytic degradation were best described by second-order kinetics. The good reusability of AgNPs was confirmed through four cycles of degradation. Additionally, phytotoxicity studies with *C. sativus* confirmed the non-toxic nature of the degraded products of RhB, a crucial aspect when considering the environmental impact of organic contaminant degradation. In conclusion, this research highlights a promising strategy for sustainable nanomaterial synthesis with significant implications for environmental and water quality management. Moreover, the success in repurposing agro-industrial waste for synthesizing AgNPs contributes to effective waste management and opens avenues for exploring other agro-wastes.

DATA AVAILABILITY STATEMENT

All relevant data are included in the paper or its Supplementary Information.

CONFLICT OF INTEREST

The authors declare there is no conflict.

REFERENCES

Abbas, A. & Amin, H. M. A. 2022 Silver nanoparticles modified electrodes for electroanalysis: An updated review and a perspective. *Microchemical Journal* **175**, 107166. https://doi.org/10.1016/j.microc.2021.107166.

Abdelghany, T. M., Al-Rajhi, A. M. H., Al Abboud, M. A., Alawlaqi, M. M., Ganash Magdah, A., Helmy, E. A. M. & Mabrouk, A. S. 2018 Recent advances in green synthesis of silver nanoparticles and their applications: About future directions. A review. *BioNanoScience* **8** (1), 5–16. https://doi.org/10.1007/s12668-017-0413-3.

Aisida, S. O., Ugwu, K., Akpa, P. A., Nwanya, A. C., Ejikeme, P. M., Botha, S., Ahmad, I., Maaza, M. & Ezema, F. I. 2019 Biogenic synthesis and antibacterial activity of controlled silver nanoparticles using an extract of *Gongronema latifolium*. *Materials Chemistry and Physics* **237**, 121859. https://doi.org/10.1016/j.matchemphys.2019.121859.

Alex, K. V., Pavai, P. T., Rugmini, R., Prasad, M. S., Kamakshi, K. & Sekhar, K. C. 2020 Green synthesized Ag nanoparticles for bio-sensing and photocatalytic applications. *ACS Omega* **5** (22), 13123–13129. https://doi.org/10.1021/acsomega.0c01136.

Ayinde, W. B., Gitari, W. M. & Samie, A. 2019 Optimization of microwave-assisted synthesis of silver nanoparticle by *Citrus paradisi* peel and its application against pathogenic water strain. *Green Chemistry Letters and Reviews* **12** (3), 225–234. https://doi.org/10.1080/17518253.2019.1627427.

Azeez, L., Lateef, A. & Olabode, O. 2023 An overview of biogenic metallic nanoparticles for water treatment and purification: The state of the art. *Water Science and Technology* **88** (4), 851–873. https://doi.org/10.2166/wst.2023.255.

Aziz, N., Faraz, M., Pandey, R., Shakir, M., Fatma, T., Varma, A., Barman, I. & Prasad, R. 2015 Facile algae-derived route to biogenic silver nanoparticles: Synthesis, antibacterial, and photocatalytic properties. *Langmuir* **31** (42), 11605–11612. https://doi.org/10.1021/acs.langmuir.5b03081.

Baran, M. F., Keskin, C., Baran, A., Hatipoğlu, A., Yildiztekin, M., Küçükaydin, S., Kurt, K., Hoşgören, H., Sarker, M. M. R., Sufianov, A., Beylerli, O., Khalilov, R. & Eftekhari, A. 2023 Green synthesis of silver nanoparticles from *Allium cepa* L. peel extract, their antioxidant, antipathogenic, and anticholinesterase activity. *Molecules* **28** (5), 1–17. https://doi.org/10.3390/molecules28052310.

Brum, B. R., Oliveira, N. R., Reis, H. C. O., Lima, Z. M. & Morais, E. B. 2016 Qualidade das águas de poços rasos em área com déficit de saneamento básico em Cuiabá, MT: Avaliação microbiológica, físico-química e fatores de risco à saúde. *Holos* **2**, 179–188. https://doi.org/10.15628/holos.2016.2714.

Castro, K. C., Cossolin, A. S., Reis, H. C. O. & Morais, E. B. 2017 Biosorption of anionic textile dyes from aqueous solution by yeast slurry from brewery. *Brazilian Archives of Biology and Technology* **60**, 1–13. http://dx.doi.org/10.1590/1678-4324-2017160101.

Dadayya, M., Thippeswamy, M. G., Shivaiah, N., Veeranna, S. H., Gurubasajar, N., Subhakar, A. & Basaiah, T. 2023 Biological potential of silver nanoparticles synthesized by an endophytic fungus *Metapochonia suchlasporia*-KUMBMDBT-23. *BioNanoScience* **13**, 1790–1816. https://doi.org/10.1007/s12668-023-01177-z.

Dixit, D., Gangadharan, D., Popat, K. M., Reddy, C. R. K., Trivedi, M. & Gadhavi, D. K. 2018 Synthesis, characterization and application of green seaweed mediated silver nanoparticles (AgNPs) as antibacterial agents for water disinfection. *Water Science and Technology* **78** (1), 235–246. https://doi.org/10.2166/wst.2018.292.

Epelle, E. I., Okoye, P. U., Roddy, S., Gunes, B. & Okolie, J. A. 2022 Advances in the applications of nanomaterials for wastewater treatment. *Environments* **9** (11), 1–27. https://doi.org/10.3390/environments9110141.

Golin, R., Barbosa, A. G., Lopes, V. C. P., Caixeta, D. S., Filho, F. C. M. d. M., Dall'oglio, E. L., de Vasconcelos, L. G. & de Morais, E. B. 2022 Decolorization of Rhodamine B by Fenton reaction using iron nanoparticles supported in Brazil nutshell biomass. *Revista Materia* **27** (3), 1–11. https://doi.org/10.1590/1517-7076-RMAT-2022-0039.

Hawar, S. N., Al-Shmgani, H. S., Al-Kubaisi, Z. A., Sulaiman, G. M., Dewir, Y. H. & Rikisahedew, J. J. 2022 Green synthesis of silver nanoparticles from *Alhagi graecorum* leaf extract and evaluation of their cytotoxicity and antifungal activity. *Journal of Nanomaterials* **2022**, 1–8. https://doi.org/10.1155/2022/1058119.

Hossain, M. A., Paul, B., Khan, K. A., Paul, M., Mamun, M. A. & Quayum, M. E. 2022 Green synthesis and characterization of silver nanoparticles by using *Bryophyllum pinnatum* and the evaluation of its power generation activities on bio-electrochemical cell. *Materials Chemistry and Physics* **282**, 125943. https://doi.org/10.1016/j.matchemphys.2022.125943.

Huq, M. A., Ashrafudoulla, M., Rahman, M. M., Balusamy, S. R. & Akter, S. 2022 Green synthesis and potential antibacterial applications of bioactive silver nanoparticles: A review. *Polymers* **14** (4), 1–22. https://doi.org/10.3390/polym14040742.

Ishak, N. A. I., Kamarudin, S. K. & Timmiati, S. N. 2019 Green synthesis of metal and metal oxide nanoparticles via plant extracts: An overview. *Materials Research Express* **6** (11), 112004.

Islam, T., Repon, M. R., Islam, T., Sarwar, Z. & Rahman, M. M. 2023 Impact of textile dyes on health and ecosystem: A review of structure, causes, and potential solutions. *Environmental Science and Pollution Research* **30** (30), 9207–9242. https://doi.org/10.1007/s11356-022-24398-3.

Jain, A., Ahmad, F., Gola, D., Malik, A., Chauhan, N., Dey, P. & Tyagi, P. K. 2020 Multi dye degradation and antibacterial potential of papaya leaf derived silver nanoparticles. *Environmental nanotechnology, Monitoring and Management* **14**, 100337. https://doi.org/10.1016/j.enmm.2020.100337.

Khane, Y., Benouis, K., Albukhaty, S., Sulaiman, G. M., Abomughaid, M. M., Al Ali, A., Aouf, D., Fenniche, F., Khane, S., Chaibi, W., Henni, A., Bouras, H. D. & Dizge, N. 2022 Green synthesis of silver nanoparticles using aqueous *Citrus limon* zest extract: Characterization and evaluation of their antioxidant and antimicrobial properties. *Nanomaterials* **12** (12), 1–20. https://doi.org/10.3390/nano12122013.

Kingslin, A., Kalimuthu, K., Laxmi Kiruthika, M., Khalifa, A. S., Nhat, P. T. & Brindhadevi, K. 2023 Synthesis, characterization and biological potential of silver nanoparticles using *Enteromorpha prolifera* algal extract. *Applied Nanoscience* **13**, 2165–2178. https://doi.org/10.1007/s13204-021-02105-x.

Korkmaz, N., Ceylan, Y., Karadağ, A., Bülbüld, A. S., Aftab, M. N., Saygılı, S. & Şen, F. 2020 Biogenic silver nanoparticles synthesized from Rhododendron ponticum and their antibacterial, antibiofilm and cytotoxic activities. *Journal of Pharmaceutical and Biomedical Analysis* **179**, 1–8. https://doi.org/10.1016/j.jpba.2019.112993.

Lakkim, V., Reddy, M. C., Pallavali, R. R., Reddy, K. R., Reddy, C. V., Inamuddin, Bilgrami, A. L. & & Lomada, D. 2020 Green synthesis of silver nanoparticles and evaluation of their antibacterial activity against multidrug-resistant bacteria and wound healing efficacy using a murine model. *Antibiotics* **9** (12), 1–22. https://doi.org/10.3390/antibiotics9120902.

Majoumouo, M. S., Sibuyi, N. R. S., Tincho, M. B., Mbekou, M., Boyom, F. F. & Meyer, M. 2019 Enhanced anti-bacterial activity of biogenic silver nanoparticles synthesized from *Terminalia mantaly* extracts. *International Journal of Nanomedicine* **14**, 9031–9046. https://doi.org/10.2147/IJN.S223447.

Manikandan, D. B., Sridhar, A., Krishnasamy Sekar, R., Perumalsamy, B., Veeran, S., Arumugam, M., Karuppaiah, P. & Ramasamy, T. 2021 Green fabrication, characterization of silver nanoparticles using aqueous leaf extract of *Ocimum americanum* (Hoary Basil) and investigation of its in vitro antibacterial, antioxidant, anticancer and photocatalytic reduction. *Journal of Environmental Chemical Engineering* **9** (1), 104845. https://doi.org/10.1016/j.jece.2020.104845.

Mare, A. D., Ciurea, C. N., Man, A., Tudor, B., Moldovan, V. & Toma, F. 2021 Enteropathogenic *Escherichia coli* – A summary of the literature. *Gastroenterology Insights* **12**, 28–40.

Mousavi, S. M., Hashemi, S. A., Ghasemi, Y., Atapour, A., Amani, A. M., Savar Dashtaki, A., Babapoor, A. & Arjmand, O. 2018 Green synthesis of silver nanoparticles toward bio and medical applications: Review study. *Artificial Cells, Nanomedicine and Biotechnology* **46** (3), S855–S872. https://doi.org/10.1080/21691401.2018.1517769.

Narayanan, M., Divya, S., Natarajan, D., Senthil-Nathan, S., Kandasamy, S., Chinnathambi, A., Alahmadi, T. A. & Pugazhendhi, A. 2021 Green synthesis of silver nanoparticles from aqueous extract of *Ctenolepis garcini* L. and assess their possible biological applications. *Process Biochemistry* **107**, 91–99. https://doi.org/10.1016/j.procbio.2021.05.008.

Nguyen, T. M. T., Huynh, T. T. T., Dang, C. H., Mai, D. T., Nguyen, T. T. N., Nguyen, D. T., Dang, V. S., Nguyen, T. D. & Nguyen, T. D. 2020 Novel biogenic silver nanoparticles used for antibacterial effect and catalytic degradation of contaminants. *Research on Chemical Intermediates* **46** (3), 1975–1990. https://doi.org/10.1007/s11164-019-04075-w.

Parthasarathy, S., Wang, X., Carr, K. R., Varahan, S., Hancock, E. B. & Hancock, L. E. 2021 Sigv mediates lysozyme resistance in *Enterococcus faecalis* via RsiV and PgdA. *Journal of Bacteriology* **203** (20), e00258-21. https://doi.org/10.1128/JB.00258-21.

Ponce, A. G., Fritz, R., del Valle, C. & Roura, S. I. 2003 Antimicrobial activity of essential oils on the native microflora of organic Swiss chard. *LWT – Food Science and Technology* **36**, 679–684. https://doi.org/10.1016/S0023-6438(03)00088-4.

Rafique, M., Sadaf, I., Rafique, M. S. & Tahir, M. B. 2017 A review on green synthesis of silver nanoparticles and their applications. *Artificial Cells, Nanomedicine and Biotechnology* **45** (7), 1272–1291. https://doi.org/10.1080/21691401.2016.1241792.

Rohaizad, A., Shahabuddin, S., Shahid, M. M., Rashid, N. M., Hir, Z. A. M., Ramly, M. M., Awang, K., Siong, C. W. & Aspanut, Z. 2020 Green synthesis of silver nanoparticles from *Catharanthus roseus* dried bark extract deposited on graphene oxide for effective adsorption of methylene blue dye. *Journal of Environmental Chemical Engineering* **8** (4), 103955. https://doi.org/10.1016/j.jece.2020.103955.

Rolim, W. R., Pelegrino, M. T., de Araújo Lima, B., Ferraz, L. S., Costa, F. N., Bernardes, J. S., Rodigues, T., Brocchi, M. & Seabra, A. B. 2019 Green tea extract mediated biogenic synthesis of silver nanoparticles: Characterization, cytotoxicity evaluation and antibacterial activity. *Applied Surface Science* **463**, 66–74. https://doi.org/10.1016/j.apsusc.2018.08.203.

Saeed, S., Iqbal, A. & Ashraf, M. A. 2020 Bacterial-mediated synthesis of silver nanoparticles and their significant effect against pathogens. *Environmental Science and Pollution Research* **27**, 37347–37356. https://doi.org/10.1007/s11356-020-07610-0.

Sangaonkar, G. M. & Pawar, K. D. 2018 *Garcinia indica* mediated biogenic synthesis of silver nanoparticles with antibacterial and antioxidant activities. *Colloids and Surfaces B: Biointerfaces* **164**, 210–217. https://doi.org/10.1016/j.colsurfb.2018.01.044.

Sasikala, A., Linga Rao, M., Savithramma, N. & Prasad, T. N. V. K. V. 2015 Synthesis of silver nanoparticles from stem bark of *Cochlospermum religiosum* (L.) Alston: An important medicinal plant and evaluation of their antimicrobial efficacy. *Applied Nanoscience* **5** (7), 827–835. https://doi.org/10.1007/s13204-014-0380-8.

Shaikh, W. A., Chakraborty, S. & Islam, R. U. 2020 Photocatalytic degradation of rhodamine B under UV irradiation using *Shorea robusta* leaf extract-mediated bio-synthesized silver nanoparticles. *International Journal of Environmental Science and Technology* **17** (4), 2059–2072. https://doi.org/10.1007/s13762-019-02473-6.

Singh, P. & Mijakovic, I. 2022 Green synthesis and antibacterial applications of gold and silver nanoparticles from *Ligustrum vulgare* berries. *Scientific Reports* **12** (1), 7902. https://doi.org/10.1038/s41598-022-11811-7.

Singh, J., Kumar, V., Singh Jolly, S., Kim, K. H., Rawat, M., Kukkar, D. & Tsang, Y. F. 2019 Biogenic synthesis of silver nanoparticles and its photocatalytic applications for removal of organic pollutants in water. *Journal of Industrial and Engineering Chemistry* **80**, 247–257. https://doi.org/10.1016/j.jiec.2019.08.002.

Singh, Y., Kaushal, S. & Sodhi, R. S. 2020 Biogenic synthesis of silver nanoparticles using cyanobacterium: *Leptolyngbya* sp. WUC 59 cell-free extract and their effects on bacterial growth and seed germination. *Nanoscale Advances* **2** (9), 3972–3982. https://doi.org/10.1039/d0na00357c.

Singh, R., Hano, C., Nath, G. & Sharma, B. 2021 Green biosynthesis of silver nanoparticles using leaf extract of *Carissa carandas* L. and their antioxidant and antimicrobial activity against human pathogenic bacteria. *Biomolecules* **11** (2), 1–11. https://doi.org/10.3390/biom11020299.

Tang, S. & Zheng, J. 2018 Antibacterial activity of silver nanoparticles: Structural effects. *Advanced Healthcare Materials* **7** (13), 1701503. https://doi.org/10.1002/adhm.201701503.

Tarannum, N., Divya & Gautam, Y. K. 2019 Facile green synthesis and applications of silver nanoparticles: A state-of-the-art review. *RSC Advances* **9** (60), 34926–34948. https://doi.org/10.1039/c9ra04164h.

U.S. EPA 1988 Lettuce root elongation (*Lactuca sativa*). In: *Protocols for short term toxicity screening of hazardous waste sites* (Greene, J. C., Bartels, C. L., Warren-Hicks, W. J., Parkhurst, B. R., Linder, G. L., Peterson, S. A. & Miller, W. E. eds.). EPA 600/3-88/029, Chicago, USA.

Viana, H. N. A. C., Sganzerla, W. G., Castro, L. E. N. & Veeck, A. P. d. L. 2023 Characterization of baru (*Dipteryx alata* Vog.) and application of its agro-industrial by-product in the formulation of cookies. *Journal of Agriculture and Food Research* **12**, 100577. https://doi.org/10.1016/j.jafr.2023.100577.

Wang, C., Cao, Y. & Wang, H. 2019 Copper-based catalyst from waste printed circuit boards for effective Fenton-like discoloration of Rhodamine B at neutral pH. *Chemosphere* **230**, 278–285. https://doi.org/10.1016/j.chemosphere.2019.05.068.

First received 22 January 2024; accepted in revised form 27 May 2024. Available online 10 June 2024